E-1141

Characterization of Si_xGe_{1-x}/Si Heterostructures for Device Applications using Spectroscopic Ellipsometry

R.M. Sieg
Electrical Engineering Department
Cleveland State University
Cleveland, Ohio 44115

S.A. Alterovitz
NASA Lewis Research Center
Cleveland, Ohio 44135

E.T. Croke and M.J. Harrell
Hughes Research Laboratories
Malibu, California 90265

M. Tanner and K.L. Wang
Electrical Engineering Department
University of California Los-Angeles
Los Angeles, California 90024

R.A. Mena
NASA Lewis Research Center
Cleveland, Ohio 44135

and
P.G. Young
Electrical Engineering Department
University of Toledo
Toledo, Ohio 43606

Abstract

Spectroscopic ellipsometry (SE) characterization of several complex Si_xGe_{1-x}/Si heterostructures prepared for device fabrication, including structures for heterojunction bipolar transistors (HBT), p-type and n-type heterostructure modulation doped field effect transistors, has been performed. We have shown that SE can simultaneously determine all active layer thicknesses, Si_xGe_{1-x} compositions, and the oxide overlayer thickness, with only a general knowledge of the structure topology needed apriori. The characterization of HBT material included the SE analysis of a Si_xGe_{1-x} layer deeply buried (600 nm) under the silicon emitter and cap layers. In the SE analysis of n-type heterostructures, we examined for the first time a silicon layer under tensile strain. We found that an excellent fit can be obtained using optical constants of unstrained silicon to represent the strained silicon conduction layer. We also used SE to measure lateral sample homogeneity, providing quantitative identification of the inhomogeneous layer. Surface overlayers resulting from prior sample processing were also detected and measured quantitatively. These results should allow SE to be used extensively as a non-destructive means of characterizing Si_xGe_{1-x}/Si heterostructures prior to device fabrication and testing.

1. Introduction

The binary alloy Si_xGe_{1-x} has been a topic of intense study for electronic device applications in recent years. A recent review of growth methods and device applications is given in reference 1. One of the most important achievements to date was the 75 GHz unity-current-gain cutoff frequency[2] (f_T) for a Si_xGe_{1-x}/Si heterojunction bipolar transistor (HBT). Additionally, a variety of p-type[3,4] and n-type[5,6] heterostructures have been reported. In the HBT device, the usual configuration is a rather thick silicon cap and emitter layers on top,[7,8] a narrow coherently strained (below 100 nm) Si_xGe_{1-x} base with $x \approx 0.8$, and a silicon collector, all grown epitaxially on a silicon substrate. In the field effect quantum well heterostructure devices, there is a marked difference between the p-type and the n-type conduction devices. A key factor in the performance of these heterostructures is the lattice mismatch between silicon and Si_xGe_{1-x}. A compressively strained Si_xGe_{1-x} layer supports quantum hole confinement, while a tensile strained silicon layer supports electron confinement.[9] Thus, in the p-type devices, the structure contains a silicon top layer, a thin coherently strained Si_xGe_{1-x} ($x \approx 0.8$) undoped conduction layer, and an epitaxial silicon buffer. In the n-type devices, the structure contains a complex Si_xGe_{1-x} buffer, usually with composition grading to achieve $x \approx 0.7$, grown on a silicon substrate. This buffer has an unstrained Si_xGe_{1-x} top layer which becomes the effective substrate for the n-type device. The active layers, from top, are a cap and a donor layer both of Si_xGe_{1-x} ($x \approx 0.65$ to 0.80), a strained silicon undoped channel conduction layer, and a Si_xGe_{1-x} buffer with a constant composition ($x \approx 0.7$). In both the n-type and the p-type devices, the thickness of the strained conduction layer is kept below the critical value[1,10] so that the layers are coherently strained.

In the research and development of such devices, it is frequently necessary to obtain estimates of the structural quality of the initial material, i.e. active layers' thicknesses, Si_xGe_{1-x} composition, and lateral sample homogeneity, prior to device fabrication. These parameters must be determined non-

destructively, since device fabrication and testing will follow. Spectroscopic ellipsometry (SE) has been successfully used to evaluate $GaAs/Al_xGa_{1-x}As$,[11] $GaAs/Al_xGa_{1-x}As/In_yGa_{1-y}As$,[12,13] and $In_xGa_{1-x}As/In_{0.52}Al_{0.48}As$[13,14] heterostructures. In these studies, the alloy compositions were estimated using the energy shift algorithm,[15] which interpolates between experimentally measured dielectric functions of discrete alloy compositions using the compositional shifts of three key spectral critical points: E_0, E_1, and E_2. This algorithm requires two items of information: a database of measured dielectric functions for discrete alloy compositions; and the critical point locations as functions of the alloy composition. Because the E_0 and E_2 critical points are usually at the edge or outside the measurement range, this algorithm is most sensitive to value of the E_1 critical point. The similar application of SE, including the energy shift algorithm, to Si_xGe_{1-x}/Si systems has been hindered by several difficulties.

First, a reliable Si_xGe_{1-x} database was not available. The only experimentally measured database was obtained by Humliček et al.[16] However, the sample compositions used in this database were not calibrated except by ellipsometry.[16] Additionally, because a rotating-analyzer ellipsometer was used for the measurements, the high wavelength, low absorption data is unreliable.[16,17,18] Accurate high wavelength modeling is essential to the analysis of thick Si_xGe_{1-x}/Si structures such as HBT structures, where only the high wavelengths can penetrate to the deep layers. A new Si_xGe_{1-x} database has recently been obtained by G.E. Jellison et al.,[17] and was successfully applied[19] to the study of $Si_{0.5}Ge_{0.5}/Si$ superlattices. This database was obtained from thick, relaxed Si_xGe_{1-x} films which were grown on silicon and germanium substrates. Samples compositions were obtained by electron microprobe and Rutherford backscattering measurements. Measurements were taken using a 2°-channel spectroscopic polarization modulation ellipsometer which accurately measures low absorption substrates. Data is available over a wide spectral range (240-840 nm).

A second problem relating to SE analysis of Si_xGe_{1-x}/Si heterostructures is

the effective modeling of compressively strained Si_xGe_{1-x} layers and tensile strained silicon layers. To date, no SE work has been done on tensile strained silicon. Considerable work has been done on compressively strained Si_xGe_{1-x} using photoreflectance[20] and SE[18,19,21,22]. Two approaches to the study of strain effects on Si_xGe_{1-x} on silicon have been followed. In the first approach, the strain effect on the critical points has been studied by directly measuring the dielectric function or its derivatives.[18,20,22] Except for one study,[22] these studies have found only an extremely weak strain effect on the E_1 critical point. This result is important, as the energy shift algorithm as applied to Si_xGe_{1-x} is also expected to be very sensitive to changes in the E_1 critical point. A strong strain effect on the E_1 location would result in the energy shift algorithm giving incorrect x values. In the second approach, the energy shift algorithm has been used to test strain effects. Recent work applying the energy shift algorithm[18,19,21] to the Si_xGe_{1-x}/Si systems showed that the composition of strained Si_xGe_{1-x} layers can be accurately determined using relaxed Si_xGe_{1-x} data. An absolute error in the value of x of 0.02 or less was obtained for a wide range of compositions: $x\approx0.9$,[21] $x\approx0.8$,[18] and $x\approx0.5$.[19] These developments establish the basis for using SE in the study of complex Si_xGe_{1-x} heterostructures, including the accurate determination of alloy composition, providing the layers are thin enough to permit sufficient light penetration.

Ellipsometry has not previously been applied to the evaluation of complex Si_xGe_{1-x}/Si heterostructures of the types typically encountered in the most common electronic Si_xGe_{1-x}/Si devices. The only complex Si_xGe_{1-x}/Si heterostructure SE studies previously reported have been two strained-layer superlattice (SLS) studies[19,21]. One of these studies[21] involved very high ($x>0.9$) Si content Si_xGe_{1-x} sublayers, while the other[19] involved SLS samples with much lower Si content ($x\approx0.5$) Si_xGe_{1-x}. In both cases, the SLS period was under 40 nm. Among the issues not addressed in previous studies are: the ability of SE to examine thick Si_xGe_{1-x}/Si structures such as those often seen in HBT samples; the ability of SE to

determine the composition of a single buried Si_xGe_{1-x} layer; simple, effective modeling of an air/Si_xGe_{1-x} layer interface for the modeling of heterostructures; and the effective modeling of the tensile strained silicon layer encountered in n-type heterostructure conduction devices. In this paper we report, for the first time, successful use of SE in the evaluation of several Si_xGe_{1-x}/Si heterostructures used in the fabrication of electronic devices, including heterostructures used for the fabrication of HBT, p-type and n-type quantum well devices. SE analysis determines the layers' thicknesses in the heterostructures and their compositions simultaneously and non-destructively. In modeling the n-type conduction channel devices, we have found that the strained silicon conduction layer can be adequately modeled using the optical constants of relaxed silicon.[23] Additionally, we have demonstrated the ability of SE to measure insulator overlayers and lateral sample homogeneity. We have shown that SE can quantitatively map layers' thickness variations across the wafer, and we have qualitatively correlated our homogeneity results with growth conditions.

2. Experimental

All samples studied were grown by molecular beam epitaxy (MBE) on silicon substrates. The p-type and HBT heterostructures were grown at 550°C and 335°C respectively at Hughes Research Laboratories using a duel e-gun Perkin-Elmer (Model 430S) Si MBE system. The wafer holder was rotated at 15 revolutions per minute to promote lateral homogeneity. The ability of this Si MBE system to grow high quality Si_xGe_{1-x}/Si heterostructures which are close to target structures was verified previously[19] by growing two 15 period $Si_{0.6}Ge_{0.6}$/Si SLS samples. These samples were analyzed by x-ray diffraction (XRD) and SE.[19] The XRD spectrum for one SLS sample obtained for (004) reflection is shown in Fig. 1. The large number of superlattice satellite peaks observable in the figure and the narrow full width at half maximum (FWHM) of each peak attest to the excellent quality of this particular superlattice. Quantitative analysis of the XRD pattern gives the superlattice period and the average germanium concentration. Using these two

numbers together with the silicon and germanium shutter opening times, an accurate absolute calibration of the silicon and germanium growth rates were obtained.

The n-type heterostructures were grown at two laboratories. The first sample was grown at University of California Los Angeles (UCLA), also in a Perkin Elmer (model 430) Si MBE system, at 550°C, with the silicon grown from an e-gun and the germanium from a Knudsen cell. During growth, the samples were rotated at a rate of up to 30 revolutions per minute. Growth rates were calibrated by growing either silicon or germanium alone and using a mechanical profilometer (Dektak) to measure the thickness on the edge of the wafer. In turn, the growth rates were used to calculate the thickness and composition of all layers. The second n-type heterostructure was treated as an unknown material, assuming growth conditions and structure similar to the UCLA sample.

SE measurements were taken with a rotating-analyzer ellipsometer (RAE) described elsewhere.[24] This instrument measures the complex reflection ratio $\rho=\tan(\Psi)e^{j\Delta}$ where $\tan(\Psi)$ and $\cos(\Delta)$ are the conventional ellipsometric parameters used to represent the amplitude and phase of ρ. 100 rotations of the analyzer were averaged for each measurement to provide greater accuracy, and a shutter was used to measure and subtract off background noise. Measurements were taken in 5 to 10 nm wavelength increments. Multiple angles-of-incidence were used, with the incident angle always near the principle angle (i.e. 73°-80°). Specific wavelength ranges and incident angles used for each sample measurement are given with the results and accompanying figures.

To obtain layer thicknesses and compositions from the measured $\tan(\Psi)$ and $\cos(\Delta)$ data, a least squares minimization was performed in which the measured SE data was fitted to an appropriate model with the quantities to be determined as variable parameters. Fit quality was defined by the mean-square-error (MSE):

$$MSE = \frac{1}{2M}\sum_{i=1}^{M}\left[(\tan(\Psi_{i,e}) - \tan(\Psi_{i,c}))^2 + (\cos(\Delta_{i,e}) - \cos(\Delta_{i,c}))^2\right]. \qquad (1)$$

where M is the number of experimental ρ measurements; $\tan(\Psi_{i,e})$ and $\cos(\Delta_{i,e})$ are the experimental parameters; and $\tan(\Psi_{i,c})$ and $\cos(\Delta_{i,c})$ are the corresponding values calculated from the model. In the present work, the model was a layered structure atop an infinite substrate, with all layers' thicknesses and Si_xGe_{1-x} layers' composition x as variable parameters. Each layer and the substrate were assumed to be homogeneous with respect to thickness and optical properties; interfaces were assumed completely abrupt; and the substrate was assumed optically infinite. The model least square fits were performed using the Marquardt algorithm[25] on a 16 bit personal computer. In addition to a minimum, the least squares fit provided 90% confidence limits.[26] These estimates take into account the gradient of the MSE near the minimum and the absolute value of the MSE, but do not take into account measurement uncertainties or model inadequacies. Thus, these estimates should only be used for comparative purposes, and do not represent absolute error estimates.

In the present work, the energy shift algorithm, which is described in detail in ref 15, was used to model the Si_xGe_{1-x} dielectric function. We used the Si_xGe_{1-x} database of ref 17 because of its wide spectral range, particularly in the infra-red, and because of its very reliable composition measurements. However, because there are systematic differences in this database between a sample grown on silicon and a sample of similar composition grown on germanium, we used here only those spectra of ref 17 obtained from films grown on silicon substrates. Optical constants of silicon were taken from ref 23. The Si_xGe_{1-x} critical point functions used were:[19]

$$E_0(x) = 0.68 + 0.44x \quad (2)$$

$$E_1(x) = 2.357 + 0.9393x \quad (3)$$

$$E_2(x) = 4.30 \quad (4)$$

where $E_0(x)$, $E_1(x)$, and $E_2(x)$ are in eV. The $E_0(x)$ function is a linear interpolation between the fundamental indirect bandgaps of silicon and germanium. The exact value of $E_0(x)$ is not important, as it is completely outside our experimental energy range. The $E_1(x)$ and $E_2(x)$ functions were obtained by

fitting the spectra of ref 17 grown on silicon substrates to critical point lineshapes.[27]

In this paper, we assumed that the dielectric functions of silicon and Si_xGe_{1-x} are not affected by doping. This assumption was based on a previously published work[28] on doping effects on the silicon dielectric function showing two important points. First, the silicon dielectric function for $\lambda \geq 400$ nm is not affected by doping up to a level of 3×10^{20} cm^{-3}. Second, the locations of critical points E_1 and E_2 change by only 1% with doping of $\sim 3.5 \times 10^{19}$ cm^{-3}, which is the highest doping encountered in the present study. Moreover, this highly doped layer was present in only one device structure, with all other layers doped below the mid 10^{18} cm^{-3} range.

3. Results and Discussion

3.1. p-type conduction heterostructure device material

Fig 2, left side, shows the nominal structure of the Hughes p-type heterostructure. Nominal structure is defined as the expected structure using growth calibrations of the silicon and germanium sources. This structure is typical[3] of materials used for p-type modulation doped field effect transistors, and is the simplest practical Si_xGe_{1-x}/Si device structure. Only the Si_xGe_{1-x} layer is under strain. In addition, the thin layers which allow significant light penetration and the accurately calibrated MBE growth system make this sample an ideal first Si_xGe_{1-x} device structure for SE analysis. The 2 nm oxide is a typical thickness for native silicon dioxide on crystalline silicon exposed to room air.

The sample was measured at 6 angles-of-incidence (73°-77°) over the spectral range 300 to 780 nm. The sample was not large enough to allow for lateral homogeneity measurements. The model for SE analysis along with numerical results of the fit are given in Fig 2, right side. Additionally, the experimental results $\tan(\Psi)$ and $\cos(\Delta)$ are plotted along with the best fit model in Fig 3. This figure shows some missing data points near 540 nm, due to the inability of RAE to accurately measure $\cos(\Delta) \approx \pm 1.0$. Because low to moderate doping does not

significantly affect the dielectric function of silicon, SE sees the three top silicon layers as a single layer with nominal thickness of 50 nm. Similarly, SE cannot differentiate between the silicon substrate and the epitaxial silicon layer above it. The result, as shown in Fig 2, right side, is a four variable parameters model: the top silicon layer thickness, Si_xGe_{1-x} layer thickness and composition x, and the oxide thickness are variables. The quality of the fit is excellent throughout the spectrum, as seen in Fig 3, and in the low value of the MSE given in Fig 2, right side. Numerical results for the SE fitted parameters given in Fig 2 are in good agreement with the nominal values. No large strain effects were detected on the $Si_{0.80}Ge_{0.20}$ dielectric function. This is shown by the excellent fit obtained using relaxed Si_xGe_{1-x} reference spectra,[17] which yielded a Si_xGe_{1-x} layer composition (x=0.812), a value very near the nominal composition. This result demonstrates that SE can provide excellent results for a simple, high quality Si_xGe_{1-x}/Si structure. It also confirms the result obtained by other researchers[18,19,21] that strained Si_xGe_{1-x} can be modeled well by the energy shift algorithm using relaxed reference spectra.

3.2. HBT material

Fig 4, left side, shows the nominal structure for the present HBT sample. This structure is a little different from a Si_xGe_{1-x} HBT structure optimized[2,8] for high frequency applications. A typical HBT would have thinner silicon cap and emitter layers (~300 to 500 nm total) and the Si_xGe_{1-x} base would be ~50 nm with a graded composition. Our sample has a thick emitter layer to test the ability of SE to provide information on a deeply buried Si_xGe_{1-x} base. The choice of a constant composition base was preferred, due to the very complex nature of the analysis required to properly model a graded Si_xGe_{1-x} layer. This sample was measured by XRD; the diffraction pattern is shown in Fig 5. In this figure, the Si substrate and Si_xGe_{1-x} peaks are readily observed. Analysis of the XRD measurement assuming a coherently strained Si_xGe_{1-x} layer, yielded a composition $x=0.830 \pm 0.002$. The nominal structure was also confirmed by secondary ion mass

spectroscopy (SIMS). A depth profile was performed. The thicknesses of the layers were estimated from the points where the germanium signal dropped to half its maximum value. The results were: silicon layer thickness, 590 ± 10 nm; and Si_xGe_{1-x} layer thickness (FWHM) 85 ± 10 nm. SE measurements were taken at 4 angles-of-incidence (74°-77°) over the wavelength range 300 to 780 nm. Because there is negligible light penetration through the silicon cap and emitter layers below 350 nm, only measurements above 350 nm were analyzed. The model used for SE along with numerical SE results for the fitted parameters are given in Fig 4, right side. Experimental results tan(Ψ) and cos(Δ) are plotted along with the best fit model in Fig 6. As with the p-type conduction device, the two topmost silicon layers, which differ only in doping concentration, were combined into a single nominally 600 nm silicon layer in the SE model. The result is a four parameter model identical to that used for the p-type conduction device, except for the nominal thicknesses. The resulting MSE given in Fig 4 is much higher than that obtained for the p-type heterostructure. This may be due to the oscillations in the measurement which were difficult to fit exactly. However, all measured oscillation peak locations were matched by the model, providing good evidence that the silicon cap/emitter layer thickness was determined accurately. Of the SE numerical results, only the silicon and Si_xGe_{1-x} layer thicknesses agree well with the nominal values, and the results of the SIMS profile. The x value of the Si_xGe_{1-x} layer is 0.032 higher than that obtained by XRD and 0.062 above the nominal value. Assuming the XRD result is accurate, the 0.032 ± 0.01 error in the SE result compared with the XRD estimate may be due to two factors: first, as noted earlier strain effects can produce an error of up to 0.02 in x. Second, the thick silicon top layers were not penetrated for light below 440 nm. Calculating $E_1(x)$ for x=0.83, the $Si_{0.83}Ge_{0.17}$ E_1 occurs at 395 nm. Because the sensitivity of the dielectric function with respect to x is greatest at photon energies at or above E_1, the shielding of the Si_xGe_{1-x} base by the silicon cap and emitter layers will greatly increase the uncertainty in x in this case. This is supported by the associated 90% confidence limit, which is 2½ times larger than the uncertainty on x obtained for any other Si_xGe_{1-x}/Si heterostructure presented

in this study. The second parameter where SE disagrees with the nominal structure is the oxide thickness, determined by SE to be 4.55 nm. This would be extremely thick for native silicon oxide. However, it was later discovered that the sample had been previously used in the first step of processing, i.e. a 150°C, 30 min dehydration bake in air, photoresist was applied and soft baked at 90°C for 30 min and then removed by acetone. Oxidation and residue resulting from this processing were detected by SE as an increase in the apparent native oxide thickness.

Because a relatively large section of the HBT structure wafer was available, three spots covering a lateral distance of 1.5 cm were measured at a fixed angle-of-incidence of 77° to examine lateral sample homogeneity. The homogeneity scans were taken immediately after the measurement of the original spot, and movement of the sample was done using an adjustment on the sample holder to minimize errors in alignment and guarantee linear movement across the sample surface. These scans, shown in Fig 7, are very similar, indicating the sample is homogenous. This is particularly important at higher wavelengths, where the base is being penetrated. Base penetration is indicated by the oscillations which begin just below 440 nm. These scans were analyzed using the model given in Fig 4. Results of all three homogeneity scans showed variations much less than the 90% confidence limits for all four variable parameters.

The experimental oscillations onset can be used to provide a decent estimate of the emitter thickness. The light penetration depth δ is given by $\delta=\lambda/4\pi k$, where λ is the wavelength and k is the extinction coefficient. As a general rule, any interface which is more than 2δ deep will not be detected by SE.[16] Calculating δ from the reference silicon data,[23] δ=292.9 nm at λ=438 nm and δ=304.5 nm at λ=440 nm. Thus, the start of oscillations just below 440 nm gives an emitter thickness estimate between 586 nm and 609 nm. This result is in good agreement with the nominal value and the SE result and, while not very precise, can be obtained with no numerical analysis.

The analysis of this sample has demonstrated that SE can be used to study HBT samples with thick cap/emitter layers, albeit with a slight decrease in

sensitivity to the Si_xGe_{1-x} base composition. We have also shown that SE can detect very thin insulator overlayers which may inadvertently result from sample processing. Clearly, this latter result can be extended to measurement of protective insulator layers intentionally deposited on the heterostructure.

3.3. n-type heterostructure device materials

Fig 8, left side, shows the nominal structure for the UCLA n-type heterostructure.[9] This structure is clearly more complicated than the p-type device presented previously. The 3.5 μm graded buffer provides an effective substrate with the same lattice constant as $Si_{0.65}Ge_{0.35}$. Of the active layers, only the 15 nm silicon conduction channel is strained. This silicon layer is under tensile strain, a topic which has not previously been studied using SE. The sample was measured by SE at five angles-of-incidence (76°-80°) over the wavelength range 320 to 640 nm. The sample was not measured above λ=640 nm to avoid significant penetration of the graded Si_xGe_{1-x} layer.

The SE model structure and numerical results for the fitted parameters are given in Fig 8, right side. In this model, all Si_xGe_{1-x} layers were assumed to have identical composition, described by a single composition parameter x. This assumption is reasonable, as all Si_xGe_{1-x} layers were grown with nominally the same composition, by the same MBE system at essentially the same time. The upper Si_xGe_{1-x} cap and spacer layers differ only in doping concentration and were combined into a single nominally 40 nm layer in the SE model. Because measurements were limited to $\lambda \leq 640$ nm, light penetration through the graded buffer should be minimal, and the 1 μm Si_xGe_{1-x} layer was taken as the effective substrate for SE analysis. At 640 nm, the light penetration depth of $Si_{0.65}Ge_{0.35}$ is δ=1.1 μm, as derived from ref 17 data. This indicates that at this wavelength, the 1 μm $Si_{0.65}Ge_{0.35}$/graded buffer interface was penetrated, but the graded buffer/Si substrate interface was not. The $Si_{0.65}Ge_{0.35}$/graded buffer interface is not a physical discontinuity, however, since the material on both sides is $Si_{0.65}Ge_{0.35}$, and so no light will reflect from it. As a result, the 15 nm

Si/1 μm $Si_{0.65}Ge_{0.35}$ interface is the deepest interface from which non-negligible light intensity will reflect, and therefore the substrate was modeled as Si_xGe_{1-x}, $x=0.65$, neglecting any contributions to the reflected light intensity from the graded layer. The strained silicon layer was modeled using the optical constants of relaxed silicon.[23] The oxide overlayer was modeled as silicon dioxide. Several researchers[17,18,20] have examined the surface of Si_xGe_{1-x} thick films and have found the surface composition and structure to be very complex. However, it is reasonable to assume the overlayer will be an insulator, and for a very thin insulator film, SE determines only the optical thickness n_od_o, where n_o is the insulator refractive index and d_o is the insulator film thickness. Thus, a small error in n_o will simply result in a corresponding small error in d_o.[29] The resulting model contains four parameters: three layer thicknesses and the Si_xGe_{1-x} composition x. The model fit was not particularly good, as shown by Fig 9. The MSE is 2½ times larger than the Hughes p-type heterostructure device measurement, the x value is 0.041 above nominal, and the Si_xGe_{1-x} thickness is 3.5 nm above nominal.

Because a quarter wafer was available, five spots, covering a lateral distance of 1.6 cm, were measured at a constant angle-of-incidence of 77°, to investigate possible lateral inhomogeneity. As with the HBT sample, the homogeneity scans were taken immediately after the original measurements shown in Fig 9. Sample movement was performed using the sample holder adjustment vernier, and one of the five spots was the same as the original spot (sample vernier 97.8) to provide a check on repeatability. The $\tan(\Psi)$ and $\cos(\Delta)$ SE homogeneity measurement data are shown in Fig 10. Comparison of Fig 10 with Fig 7, the Hughes HBT homogeneity scans over a similar lateral distance, shows that the UCLA n-type heterostructure device has much more lateral inhomogeneity. Lateral inhomogeneity was particularly important for our SE measurements, because the large experimental angles-of-incidence result in the probe beam covering a large surface area. Also, there was a significant difference in surface area probed between the 76° and 80° angle-of-incidence scans. Thus the large MSE

shown in Fig 8 can be traced to the inhomogeneity of this sample, together with the analysis including all scans in the range 76°-80°. For this reason, we re-analyzed the original measurement (at vernier 97.8) using only the 77° scan, and also analyzed each of the five homogeneity scans, all using the same model given in Fig 8, right side. Results of these fits are shown in Table I. The fits obtained here were generally much better than the five angle-of-incidence fit given in Fig 8, except near the edge of the wafer (vernier=34.0), as shown by the MSE. Results of both measurements taken at vernier=97.8 (near the wafer center) given in Table I, and also the 5 angles-of-incidence fit shown in Fig 8 (which was also measured at vernier=97.8) yield very similar parameter values. Table I shows that, as the SE light probe beam spot moves from the wafer center (vernier 97.8) to the wafer edge (vernier 34.0), the Si layer thickness remains constant within the experimental 90% confidence limits, while the Si_xGe_{1-x} layer thickness decreases by 3.0 nm. The Si_xGe_{1-x} layer thickness is plotted as a function of the scan location (given by the sample vernier) in Fig 11. A nearly linear thickness gradient is seen. Further discussions with the grower at UCLA provided an explanation for these layer thickness gradients. The silicon e-gun source is located at an angle ~10° from the sample normal, while the germanium Knudsen cell is ~30° from the sample normal in the opposite direction and slightly nearer to the wafer. These location differences should result in a Si_xGe_{1-x} thickness inhomogeneity, with a thicker film at the wafer center (even after sample rotation), in excellent agreement with the SE measurements. Table I also shows that the edge scan (vernier=34.0) agrees most closely with the nominal profilometer values. This is because, as mentioned earlier, this MBE system was calibrated using profilometry measurements taken near the edge of the wafer, where the sample holder leaves an unexposed portion of the substrate from which the film thickness can be measured. The nominal values were calculated from this calibration, and so they were most accurate near the wafer edge, where the calibration was done.

We have demonstrated several items with this sample analysis. First, we have shown that the tensile strained silicon conduction layer can be adequately

modeled using unstrained silicon optical constants. This strongly indicates that the silicon dielectric function is not significantly affected by tensile strain, as was previously shown for Si_xGe_{1-x} under compressive strain.[18,19,21] Second, we have shown the SE can obtain specific, quantitative information on Si_xGe_{1-x}/Si heterostructure lateral inhomogeneity. The results given here using five scans on a quarter wafer could easily be extended to a complete wafer mapping using many scans. The result shown in Fig 11 shows the quantitative nature of the lateral homogeneity scans and is an extension of the lateral wafer homogeneity study previously performed by SE on GaAs/Al_xGa_{1-x}As heterostructures.[30] Unlike the GaAs/Al_xGa_{1-x}As study, in which the samples were extremely homogenous, here we successfully obtained quantitative results on an inhomogeneous heterostructure. We have also shown that a simple silicon dioxide overlayer, which adds one parameter to the model, satisfactorily models the exposed Si_xGe_{1-x} surface. In fact, the oxide thickness obtained, 2.5-3.0 nm, is very similar to a typical native silicon dioxide layer on silicon.

Because the UCLA n-type conduction device was inhomogeneous, we still wanted to measure a high quality, homogenous n-type heterostructure material. We also decided not to obtain detailed structural information about this material, so as to test our SE technique. A second sample was supplied by UCLA, but was made in another growth chamber. The sample growth method and structure were not known, but were believed[9] to be similar to the UCLA n-type heterostructure material presented previously. The SE measurements were taken at six angles-of-incidence (74°-79°) over the wavelength range 300 to 800 nm. This sample was too small to allow for lateral homogeneity measurements. The sample was analyzed using the same model used for the UCLA sample (Fig 8). The fit was reasonably good; however, clear systematic errors were seen at high wavelengths. For this reason, we re-analyzed the measurement, fitting data only in the spectral range 300 to 600 nm to avoid penetrating the graded layer/silicon substrate interface. An excellent fit was obtained for this restricted wavelength range. Numerical results of the fitted parameters are given in Table II, and the measurement and model are plotted in Fig 12. All parameter values appear reasonable for an n-

type conduction device, except the oxide. The very thick oxide obtained is almost certainly due to residue left over from our own previous sample processing, when an antimony contact layer was etched off. The MSE is the lowest obtained for any Si_xGe_{1-x}/Si heterostructure presented in this paper. In this last sample analysis, we have demonstrated again the ability of SE to provide an excellent fit for a high quality Si_xGe_{1-x} heterostructure, this time an n-type conduction device with only an approximate knowledge of its nominal structure. Also, as with the HBT, we have shown that SE can detect and quantitatively measure the effects of sample processing, in this case an antimony etch.

4. Conclusions

In conclusion, we have successfully applied SE to the analysis of structures used in the most common electronic Si_xGe_{1-x}/Si devices. We have shown that SE can provide all the active layers' thicknesses, the Si_xGe_{1-x} layers' compositions, and the insulator overlayer thickness, using simple (e.g. four parameter) models and a data inversion algorithm which can be executed on a 16 bit personal computer. We have also shown that SE can be used to study wafer homogeneity, demonstrating for the first time that SE can quantitatively map lateral inhomogeneity of specific layer thicknesses across the wafer. In analyzing the two n-type heterostructures, we have applied SE to tensile strained silicon for the first time. We found that the strained silicon layer can be represented by the optical constants of relaxed silicon, showing that the dielectric function of silicon is relatively unaffected by the tensile strain. We have also shown that the air/Si_xGe_{1-x} layer interface can be adequately modeled by a thin 2-3 nm silicon dioxide overlayer. In the analysis of the HBT structure, we have shown that SE can be used to analyze thick (~600 nm total) silicon cap/emitter layers, albeit with a slight decrease in the sensitivity to the Si_xGe_{1-x} base composition. We also observed that SE can be used to obtain a rough estimate of the net cap/emitter thickness without numerically inverting the SE data. These results should allow SE to be applied extensively as an optical non-destructive means of evaluating Si_xGe_{1-x}/Si heterostructures.

Acknowledgements

The authors would like to thank G.E. Jellison for providing a diskette of his Si_xGe_{1-x} database, L.D. Warren for assisting with the XRD measurements, Ya.-Hong Xie for providing the second n-type heterostructure sample, and to Charles Evans and Associates for the SIMS results.

References

1. J.C. Bean, Proc. IEEE, 80, 571 (1992).
2. G.L. Patton, J.H. Comfort, B.S. Meyerson, E.F. Crabbe, G.J. Scilla, E. De-Fresart, J.M.C. Stork, J.Y.-C. Sun, D.L. Harame, and J.N. Burghartz, IEEE Elec. Dev. Lett., EDL-11, 171 (1990).
3. T.P. Pearsall and J.C. Bean, IEEE Elec. Dev. Lett., EDL-7, 308 (1986).
4. D.K. Nayak, J.C.S. Woo, J.S. Park, K.-L. Wang, and K.P. MacWilliams, IEEE Elec. Dev. Lett. EDL-12, 154 (1991).
5. U. Konig, A.J. Boers, F. Schaffler, and E. Kasper, Elec. Lett. 28, 160 (1992).
6. K. Ismail, B.S. Meyerson, S. Rishton, J. Chu, S. Nelson, and J. Nocera, IEEE Elec. Dev. Lett., EDL-13, 229 (1992).
7. C.A. King, J.L. Hoyt, and J.F. Gibbons, IEEE Elec. Dev., ED-36, 2093 (1989).
8. A. Gruble, H. Kibbel, U. Konig, U. Erban, and E. Kasper, IEEE Elec. Dev. Lett., EDL-13, 206 (1992).
9. Y.J. Mii, Y.H. Xie, E.A. Fitzgerald, Don Monroe, F.A. Thiel, B.E. Weir, and L.C. Feldman, Appl. Phys. Lett., 59, 1611 (1991).
10. Y. Kohama, Y. Fukuda, and M. Seki, Appl. Phys. Lett. 52, 380 (1988).
11. P.G. Snyder, M.C. Rost, G.H. Bu-Abbud, J.A. Woollam, and S.A. Alterovitz, J. Appl. Phys., 60, 3293 (1986).
12 S.A. Alterovitz, P.A. Sekula-Moise, R.M. Sieg, M.N. Drotos, and N.A. Bogner, Thin Solid Films, in print.
13 S.A. Alterovitz, R.M. Sieg, H.D. Yao, P.G. Snyder, J.A. Woollam, J. Pamulapati, P.K. Bhattacharya, and P.A. Sekula- Moise, Thin Solid Films, 206, 288 (1991).
14 S.A. Alterovitz, R.M. Sieg, J. Pamulapati, and P.K. Bhattacharya, to be published.
15. P.G. Snyder, J.A. Woollam, S.A. Alterovitz, and B. Johs, J. Appl. Phys. 68, 5925 (1990).
16. J. Humliček, M. Garriga, M.I. Alonso, and M. Cardona, J. Appl. Phys., 65,

2827 (1989).

17. G.E. Jellison, T.E. Haynes, and H.H. Burke, Opt. Mat., to be published.
18. C. Pickering, R.T. Carline, D.J. Robbins, W.Y. Leong, S.J. Barnett, A.D. Pitt, and A.G. Cullis, J. Appl. Phys., to be published.
19. R.M. Sieg, S.A. Alterovitz, E.T. Croke, and M.J. Harrell, to be published.
20. Y. Yin, F.H. Pollak, P. Auvray, D. Dutartre, R. Pantel, and J.A. Chroboczek, Thin Solid Films, to be published.
21. H.D. Yao, J.A. Woollam, P.J. Wang, M.J. Tejwani, and S.A. Alterovitz, Applied Surface Science, to be published.
22. F. Ferrieu, F. Beck, and D. Dutartre, Solid State Comm., 82, 427 (1992).
23. G.E. Jellison, Opt. Mat. 1, 41 (1992).
24. S.A. Alterovitz, R.M. Sieg, N.S. Shoemaker, and J.J. Pouch, Mat. Res. Soc. Symp. Proc., 152, 21 (1989).
25. D.W. Marquardt, J. Soc. Indust. Appl. Math., 11, 431 (1963).
26. D.E. Aspnes, SPIE 276, 188 (1981).
27. P. Lautenschlager, M. Garriga, L. Viña, and M. Cardona, Phys. Rev., B36, 4821 (1987).
28. D.E. Aspnes, A.A. Studna, and E. Kinsbron, Phys. Rev., B29, 768 (1984).
29. H. Arwin and D.E. Aspnes, Thin Solid Films, 113, 101 (1984).
30. S.A. Alterovitz, P.G. Snyder, K.G. Merkel, J.A. Woollam, D.C. Radulescu, and L.F. Eastman, J. Appl. Phys., 63, 5081 (1988).

Figure Captions

Fig 1. XRD measurement of a calibration SLS sample. The SLS period and average germanium composition are derived from these (004) reflection data. θ is the reflection angle.

Fig 2. Nominal structure (left) and SE model and results (right) for the p-type conduction heterostructure device. x is the silicon concentration in the Si_xGe_{1-x} layer.

Fig 3. SE measurement (symbols) and best fit model (lines) for (a) $\tan(\Psi)$, and (b) $\cos(\Delta)$, of the p-type heterostructure device.

Fig 4. Nominal structure (left) and SE model and results (right) of the HBT sample. x is the silicon concentration of the Si_xGe_{1-x} layer.

Fig 5. XRD measurement of the HBT sample using the (004) reflection. θ is the reflection angle. The left peak is due to the coherently strained Si_xGe_{1-x} layer, and the right peak is due to the silicon substrate.

Fig 6. SE measurement and best fit model for (a) $\tan(\Psi)$, and (b) $\cos(\Delta)$, of the HBT sample. Because of the large number of measurements taken to accurately determine the oscillations, both the measurement and the model are shown as lines in this figure.

Fig 7. SE measurements of the HBT sample taken at several surface locations showing excellent lateral sample homogeneity: (a) tan(Ψ), and (b) cos(Δ). Legend gives sample vernier reading: 100 tics = 2.54 cm. Insert shows approximate measurement locations. Angle of incidence: 77°.

Fig 8. Nominal structure (left), and SE model and results (right), for the UCLA n-type heterostructure. The Si_xGe_{1-x} composition is nominally identical for all layers. x is the silicon concentration in both Si_xGe_{1-x} layers.

Fig 9. SE measurements (points) versus best fit model (lines) for (a) tan(Ψ), and (b) cos(Δ), of the UCLA n-type heterostructure device.

Fig 10. SE measurements of the UCLA n-type heterostructure device taken at several locations on the wafer: (a) tan(Ψ), (b) cos(Δ). Legend gives sample vernier reading: 100 tics = 2.54 cm. 34.0 is near the edge of the wafer; 97.8 is near the wafer center. Insert shows approximate measurement locations. Angle of incidence: 77°.

Fig 11. Si_xGe_{1-x} cap thickness profile for UCLA n-type heterostructure device, calculated from analysis of homogeneity scans of Fig 10 and the 77° measurement of Fig 9. Vernier Reading: 100 tics = 2.54 cm. 30 is near the edge of the wafer; 100 is near the wafer center.

Fig 12. SE measurement (symbols) and best fit model (lines) for (a) tan(Ψ), and (b) cos(Δ), of the second n-type heterostructure device.

Sample Vernier	Oxide (nm)	Si_xGe_{1-x} (nm)	Si (nm)	Si_xGe_{1-x} x	MSE $x10^{-4}$
97.8	3.00 ±.10	43.2 ±.29	13.7 ±.47	.6810 ±.0048	4.46
97.8	3.02 ±.10	43.2 ±.29	13.6 ±.48	.6809 ±.0049	4.74
79.0	2.91 ±.09	42.5 ±.27	13.9 ±.45	.6827 ±.0045	4.01
60.0	2.89 ±.10	41.6 ±.31	14.0 ±.52	.6815 ±.0050	4.98
47.0	2.81 ±.12	41.1 ±.40	14.1 ±.66	.6805 ±.0063	7.73
34.0	2.56 ±.19	40.3 ±.63	14.7 ±1.07	.6707 ±.0108	19.4

Table I. Results of SE analyses of UCLA n-type conduction device homogeneity scans shown in Fig 10 using SE model shown in Fig 8, right side. The topmost 97.8 vernier scan is the 77° scan shown in Fig 9. Vernier reading: 100 tics = 2.54 cm; 34.0 is near the wafer edge; 97.8 is near the wafer center.

Layer/Composition	Parameter Value	90% Conf. Limit
Oxide	5.60	.046
Si_xGe_{1-x} Thickness	62.0	.190
Si Thickness	16.1	.334
Composition x	.7704	.003
Trig MSE	3.79×10^{-4}	-

Table II. Results of SE analysis of an n-type heterostructure device. The nominal structure of this device is unknown. $\lambda \leq 600$ nm fitted using model of Fig 8. Thicknesses are in nm.

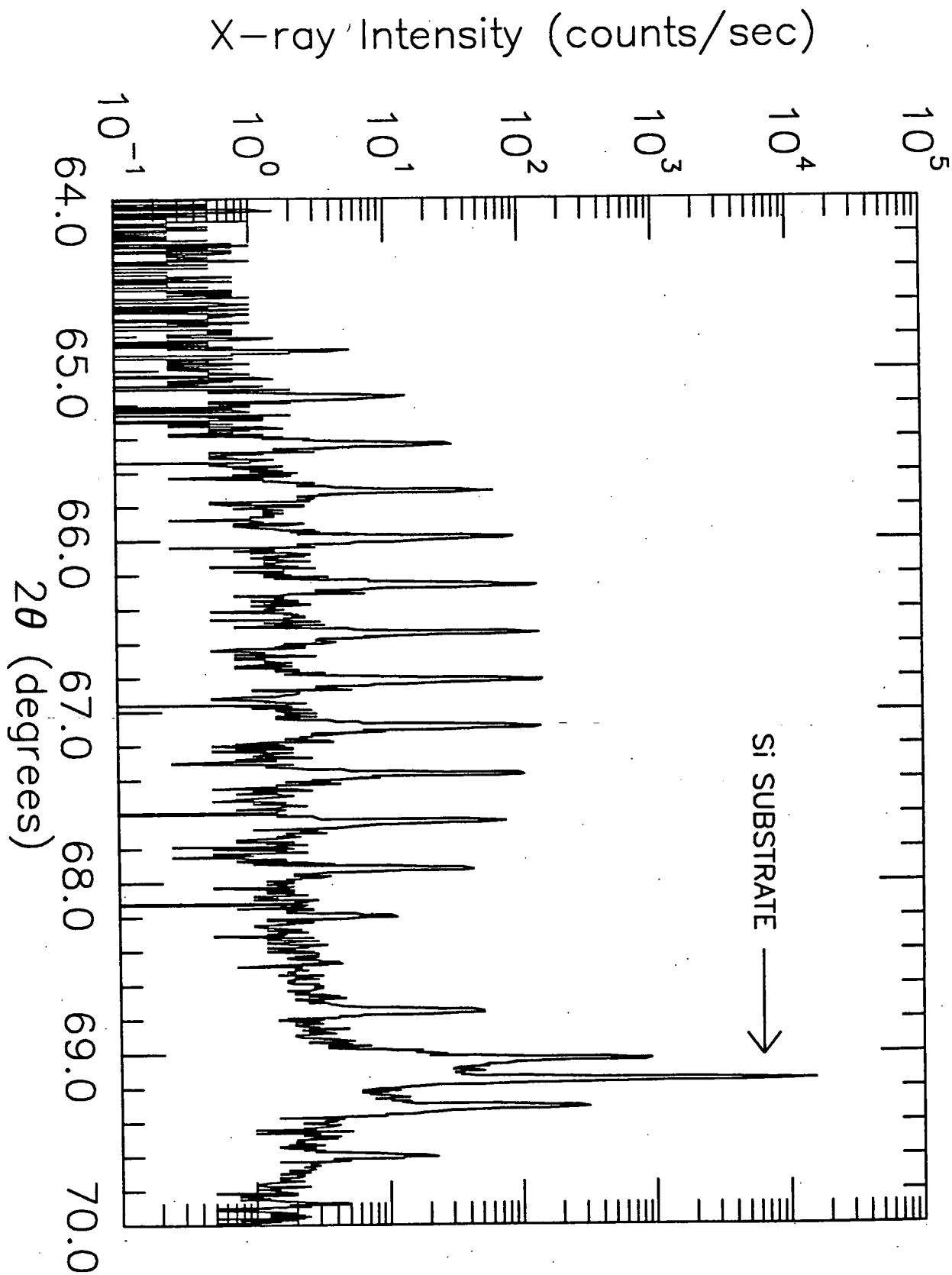
X-ray Intensity (counts/sec)
10^{-1}
10^{0}
10^{1}
10^{2}
10^{3}
10^{4}
10^{5}
64.0
65.0
66.0
67.0
68.0
69.0
70.0
2θ (degrees)
Si SUBSTRATE

Fig 1

	NOMINAL	ELLIPSOMETRY	
2 nm	Oxide	Oxide	2.28 ± 0.04 nm
20 nm	Si		
20 nm	Si:B 3.5×10^{18} cm^{-3}	Si	49.2 ± 0.29 nm
10 nm	Si		
25 nm	Si_xGe_{1-x}	Si_xGe_{1-x}	23.0 ± 0.59 nm
100 nm	Si	Si	substrate
—	Si substrate p^-	$x = 0.812 \pm 0.003$	
	$x = 0.80$	MSE: 8.42×10^{-4}	

Fig 2

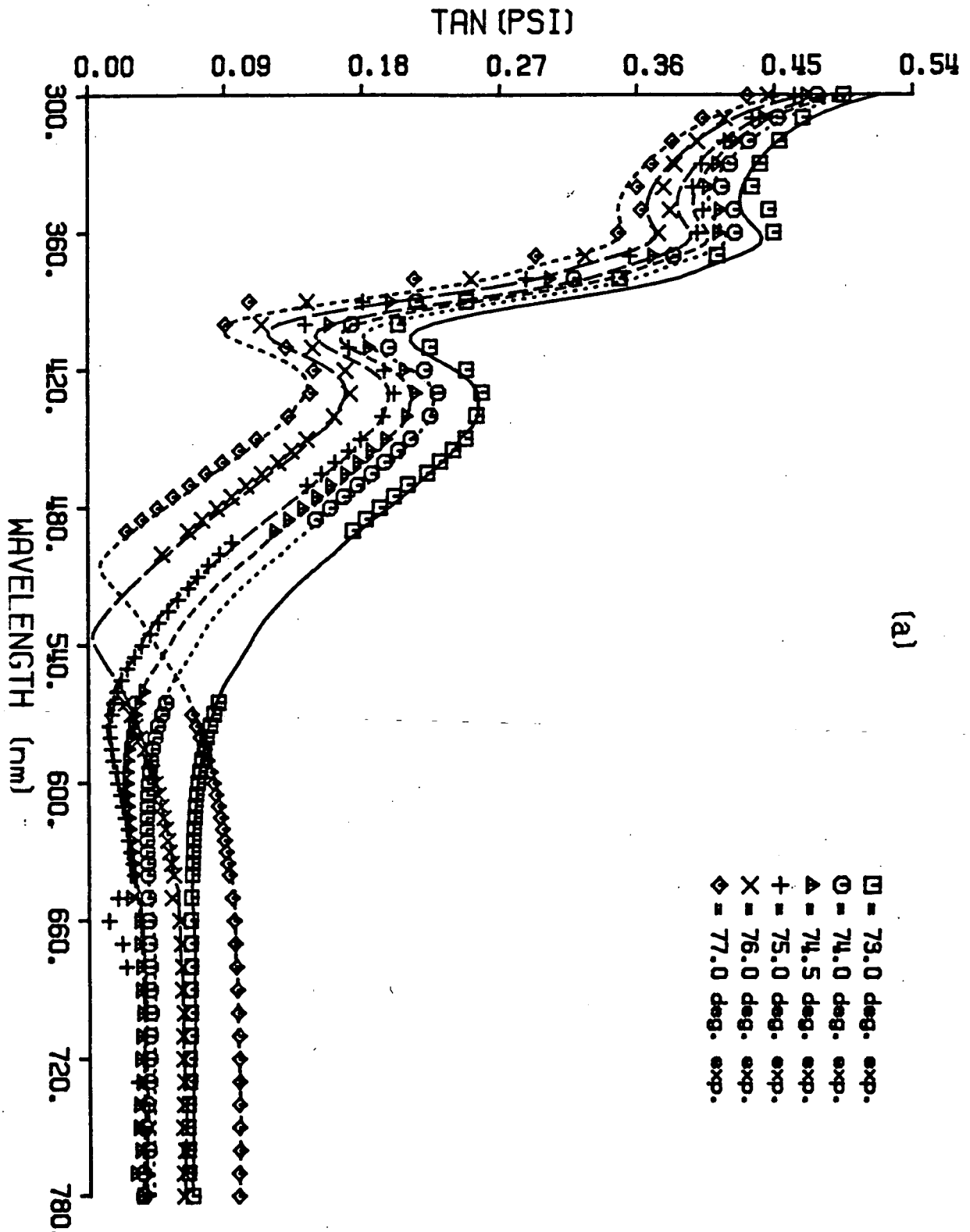
TAN (PSI)
0.00
0.09
0.18
0.27
0.36
0.45
0.54
300.
360.
420.
480.
540.
600.
660.
720.
780.
WAVELENGTH (nm)
□ = 73.0 deg. exp.
○ = 74.0 deg. exp.
▲ = 74.5 deg. exp.
+ = 75.0 deg. exp.
× = 76.0 deg. exp.
◇ = 77.0 deg. exp.
(a)

Fig 3a

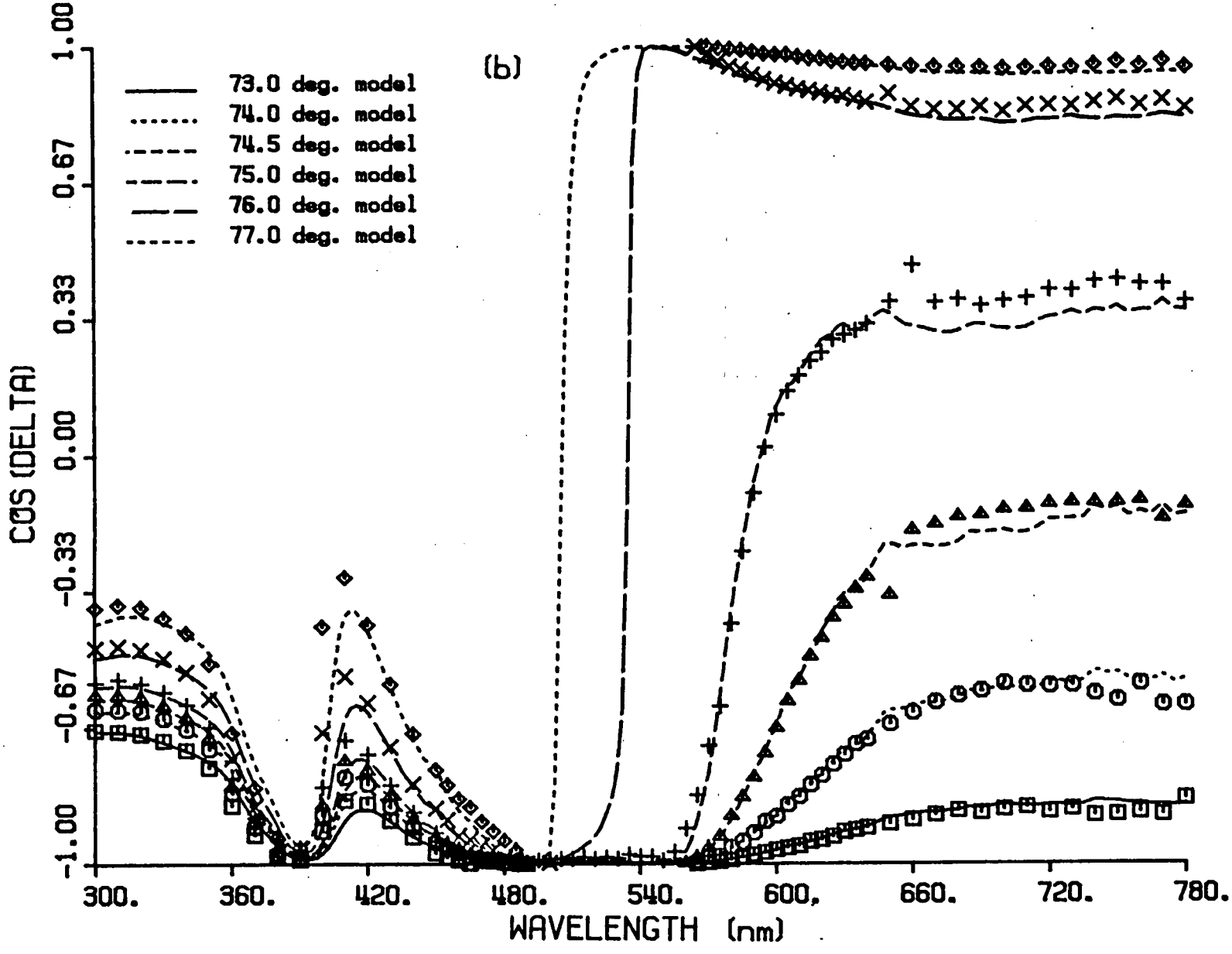
(b)
73.0 deg. model
74.0 deg. model
74.5 deg. model
75.0 deg. model
76.0 deg. model
77.0 deg. model
COS (DELTA)
1.00
0.67
0.33
0.00
-0.33
-0.67
-1.00
300.
360.
420.
480.
540.
600.
660.
720.
780.
WAVELENGTH (nm)

Fig 3b

NOMINAL		ELLIPSOMETRY	
2 nm	Oxide	Oxide	4.55 ± 0.07 nm
120 nm	Si n^{++} 2×10^{19} Sb	Si	594.3 ± 0.75 nm
480 nm	Si n^{+} 2×10^{18} Sb		
92.3 nm	Si_xGe_{1-x}	Si_xGe_{1-x}	88.5 ± 0.97 nm
	Si 1×10^{17} Sb	Si	substrate
——	Si substrate p^-	$x = 0.862 \pm 0.008$	
	$x = 0.80$	MSE: 2.07×10^{-3}	

Fig 4

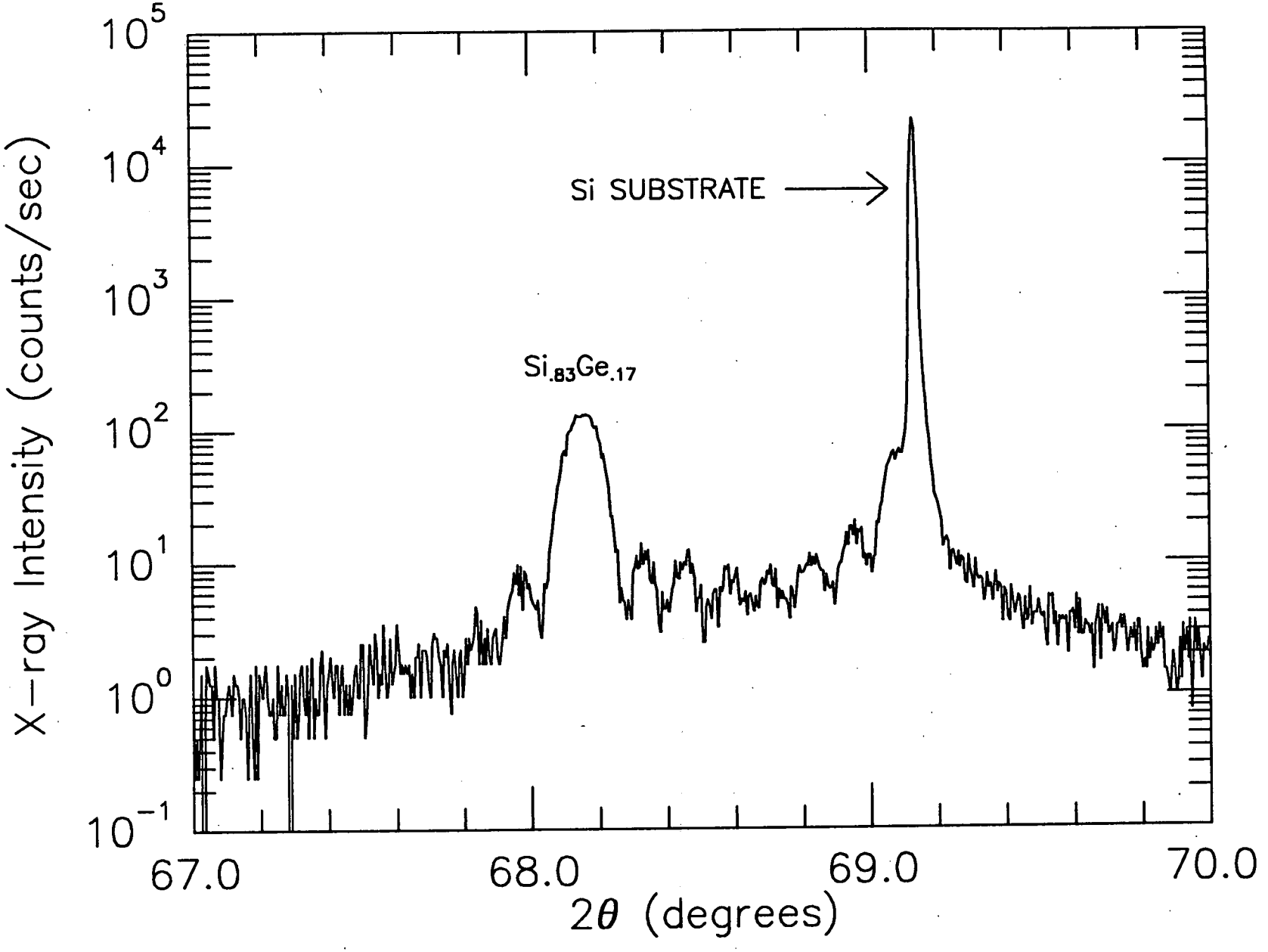
Si SUBSTRATE
$Si_{.83}Ge_{.17}$
X-ray Intensity (counts/sec)
10^5
10^4
10^3
10^2
10^1
10^0
10^{-1}
67.0
68.0
69.0
70.0
2θ (degrees)

Fig 5

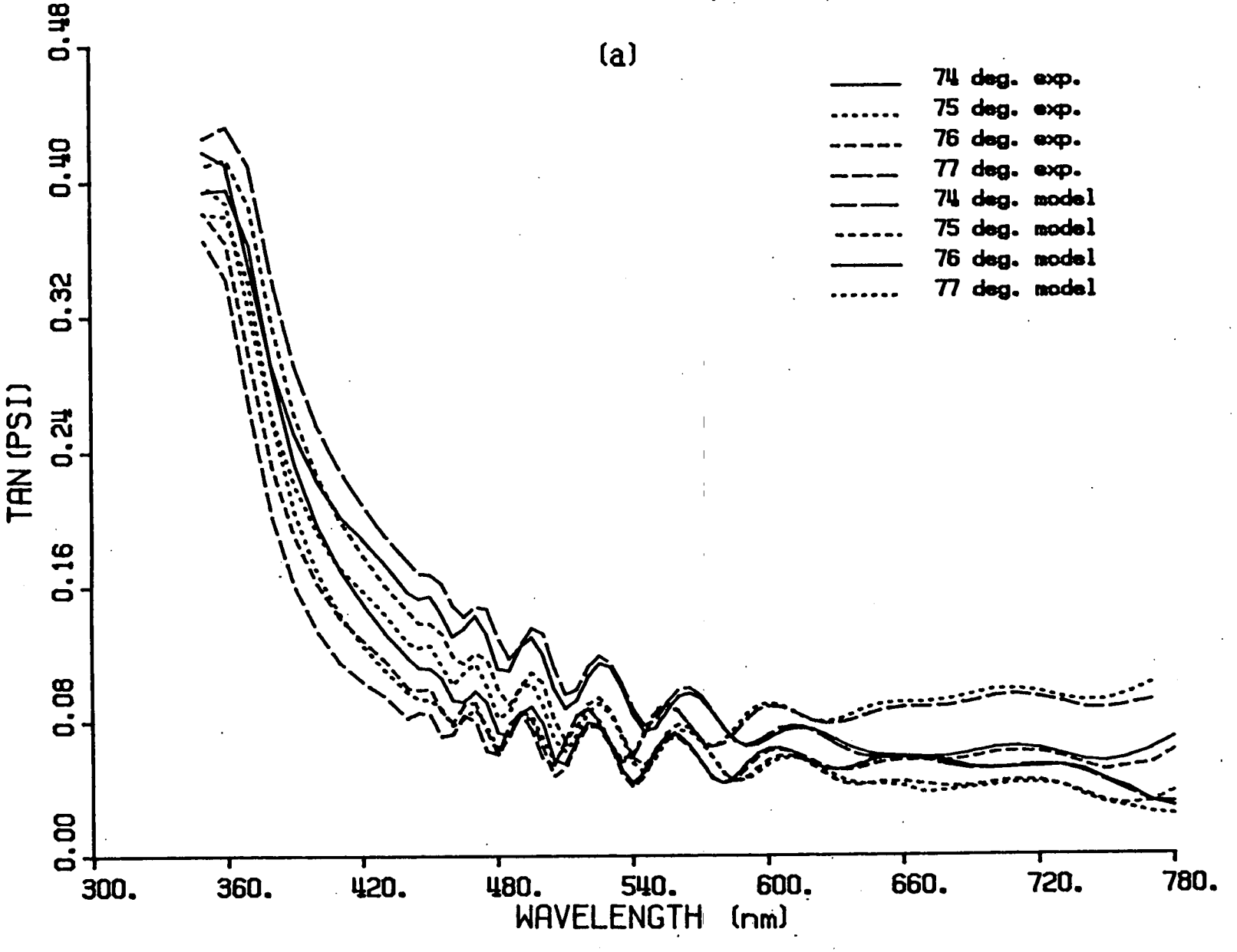
(a)
74 deg. exp.
75 deg. exp.
76 deg. exp.
77 deg. exp.
74 deg. model
75 deg. model
76 deg. model
77 deg. model
TAN (PSI)
0.00
0.08
0.16
0.24
0.32
0.40
0.48
300.
360.
420.
480.
540.
600.
660.
720.
780.
WAVELENGTH (nm)

Fig 6a

COS (DELTA)
-1.00
-0.67
-0.33
0.00
0.33
0.67
1.00
300.
360.
420.
480.
540.
600.
660.
720.
780.
WAVELENGTH (nm)
exp. 74 deg.
exp. 75 deg.
exp. 76 deg.
exp. 77 deg.
model 74 deg.
model 75 deg.
model 76 deg.
model 77 deg.
(b)

Fig 6b

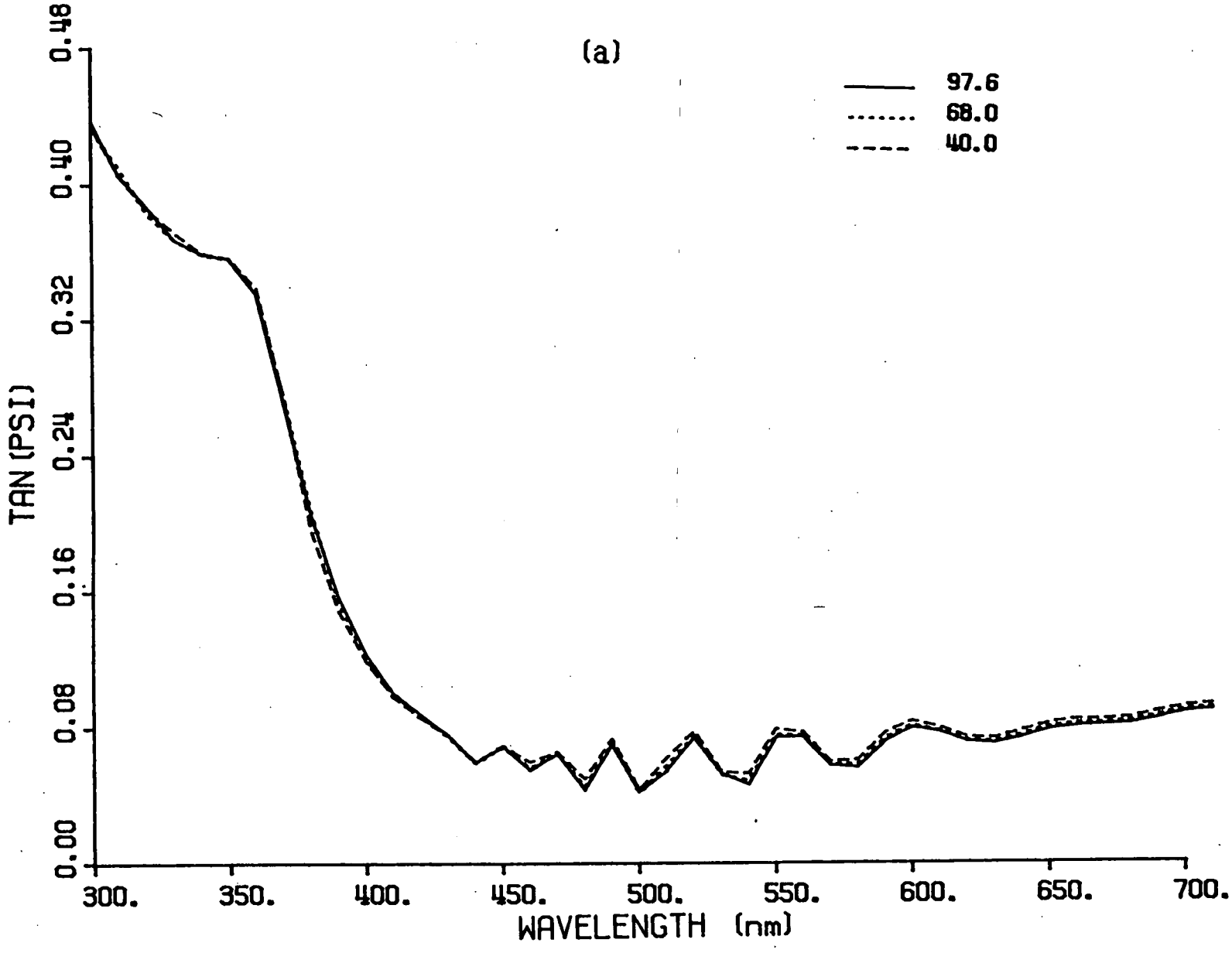
(a)
97.6
68.0
40.0
TAN (PSI)
0.00
0.08
0.16
0.24
0.32
0.40
0.48
300.
350.
400.
450.
500.
550.
600.
650.
700.
WAVELENGTH (nm)

Fig 7a

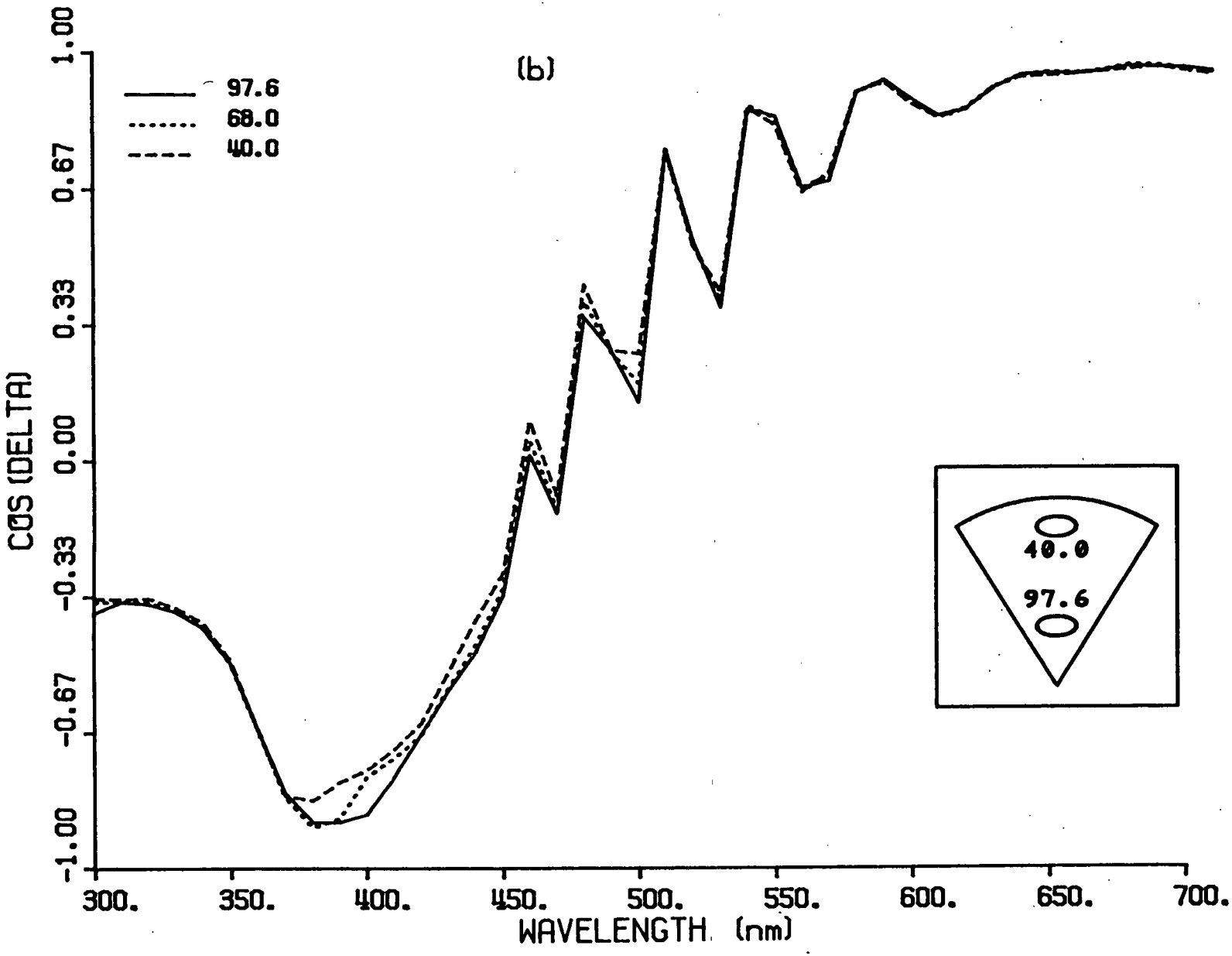
(b)
97.6
68.0
40.0
COS (DELTA)
1.00
0.67
0.33
0.00
-0.33
-0.67
-1.00
300.
350.
400.
450.
500.
550.
600.
650.
700.
WAVELENGTH (nm)
40.0
97.6

Fig 7b

NOMINAL		ELLIPSOMETRY	
2 nm	Oxide	Oxide	2.66 ± 0.09 nm
30 nm	Si_xGe_{1-x} n^+ 10^{18}	Si_xGe_{1-x}	43.5 ± 0.26 nm
10 nm	Si_xGe_{1-x}		
15 nm	Si	Si	13.1 ± 0.39 nm
1 um	Si_xGe_{1-x}	Si_xGe_{1-x} substrate	
3.5 um	graded buffer	$x = 0.691 \pm 0.003$	
—	Si substrate p^-	MSE: 2.04×10^{-3}	
$x=0.65$,	all Si_xGe_{1-x} layers		

Fig 8

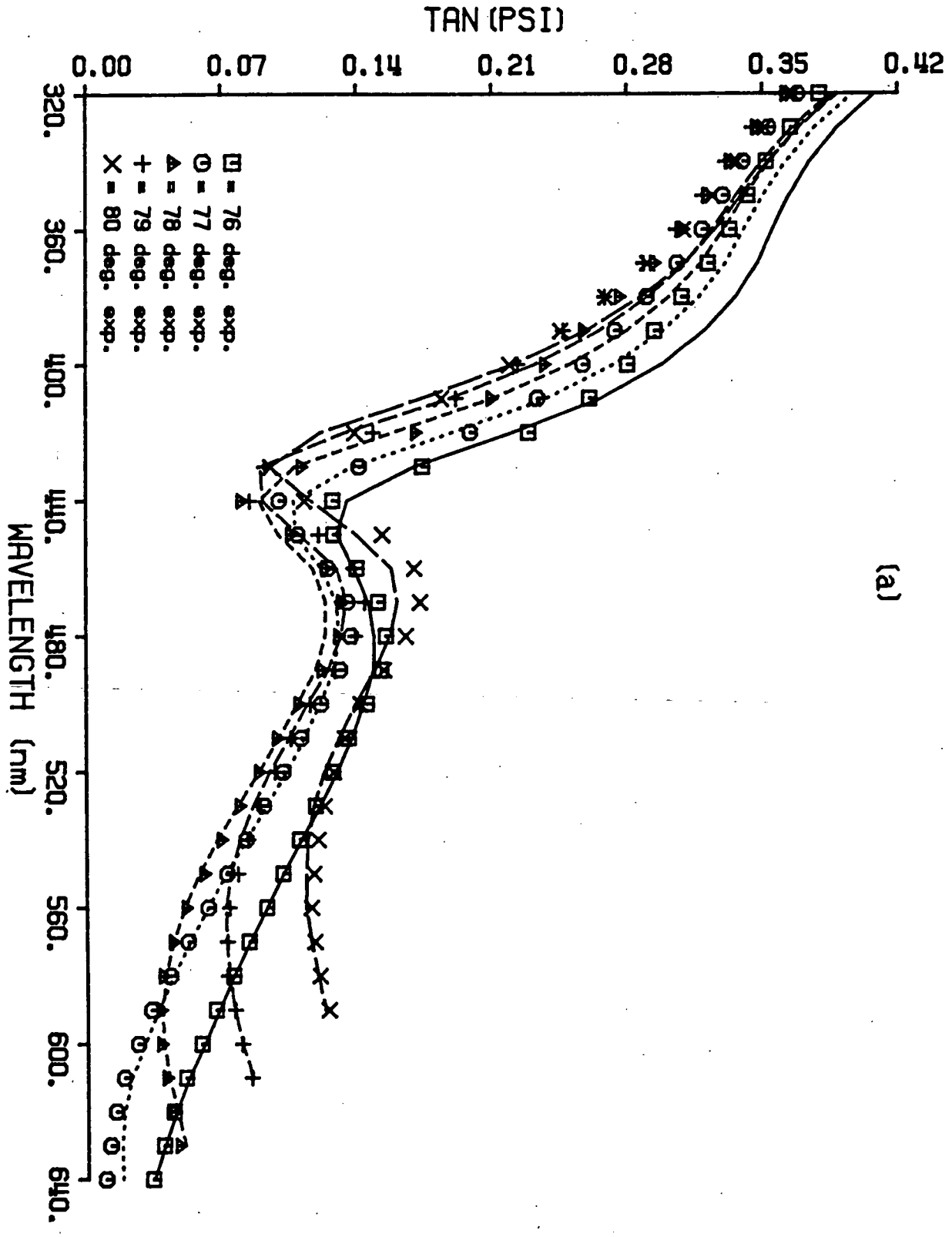
TAN (PSI)
0.00
0.07
0.14
0.21
0.28
0.35
0.42
320.
360.
400.
440.
480.
520.
560.
600.
640.
WAVELENGTH (nm)
76 deg. exp.
77 deg. exp.
78 deg. exp.
79 deg. exp.
80 deg. exp.
(a)

Fig 3a

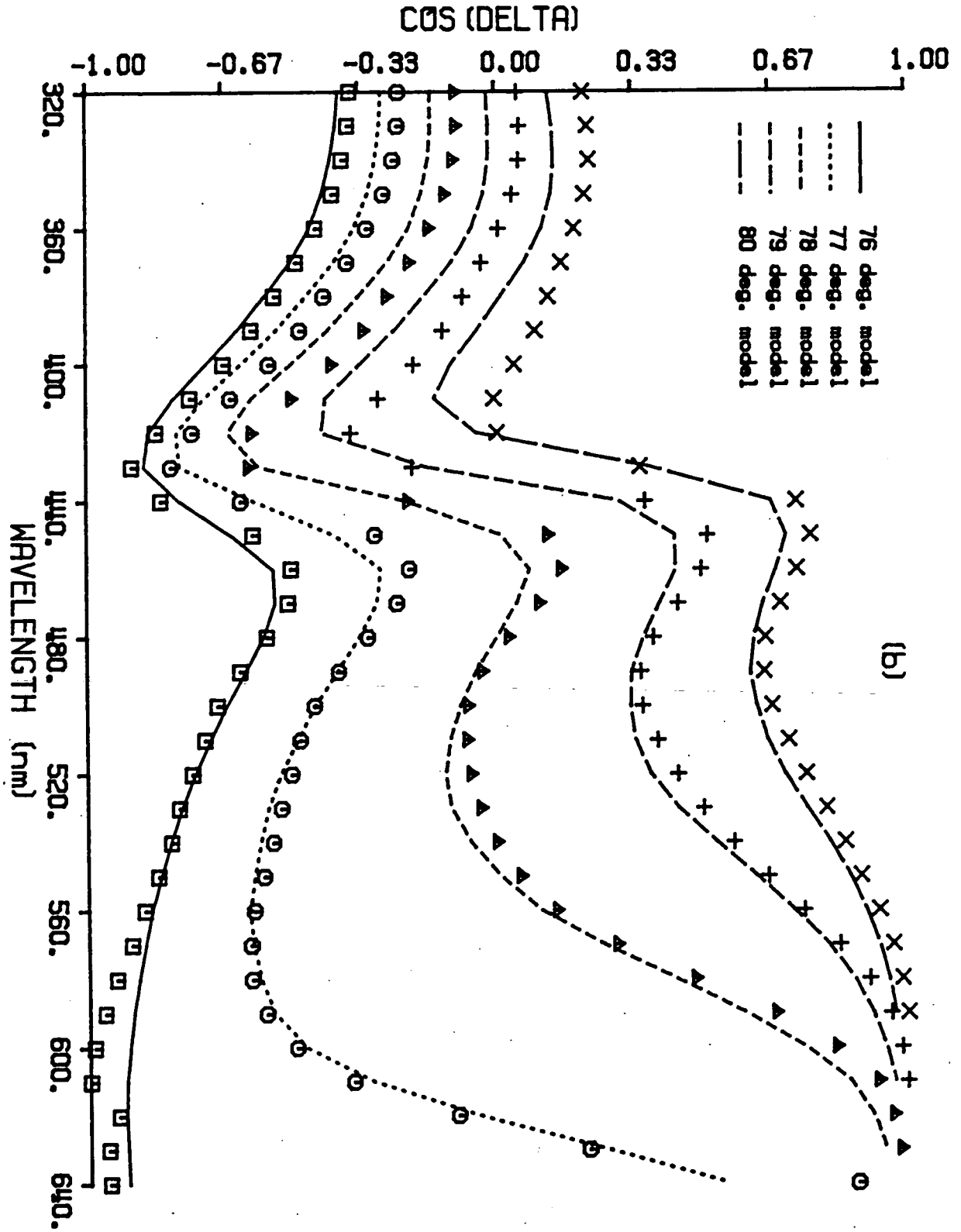
COS (DELTA)
-1.00
-0.67
-0.33
0.00
0.33
0.67
1.00
320.
360.
400.
440.
480.
520.
560.
600.
640.
WAVELENGTH (nm)
76 deg. model
77 deg. model
78 deg. model
79 deg. model
80 deg. model
(b)

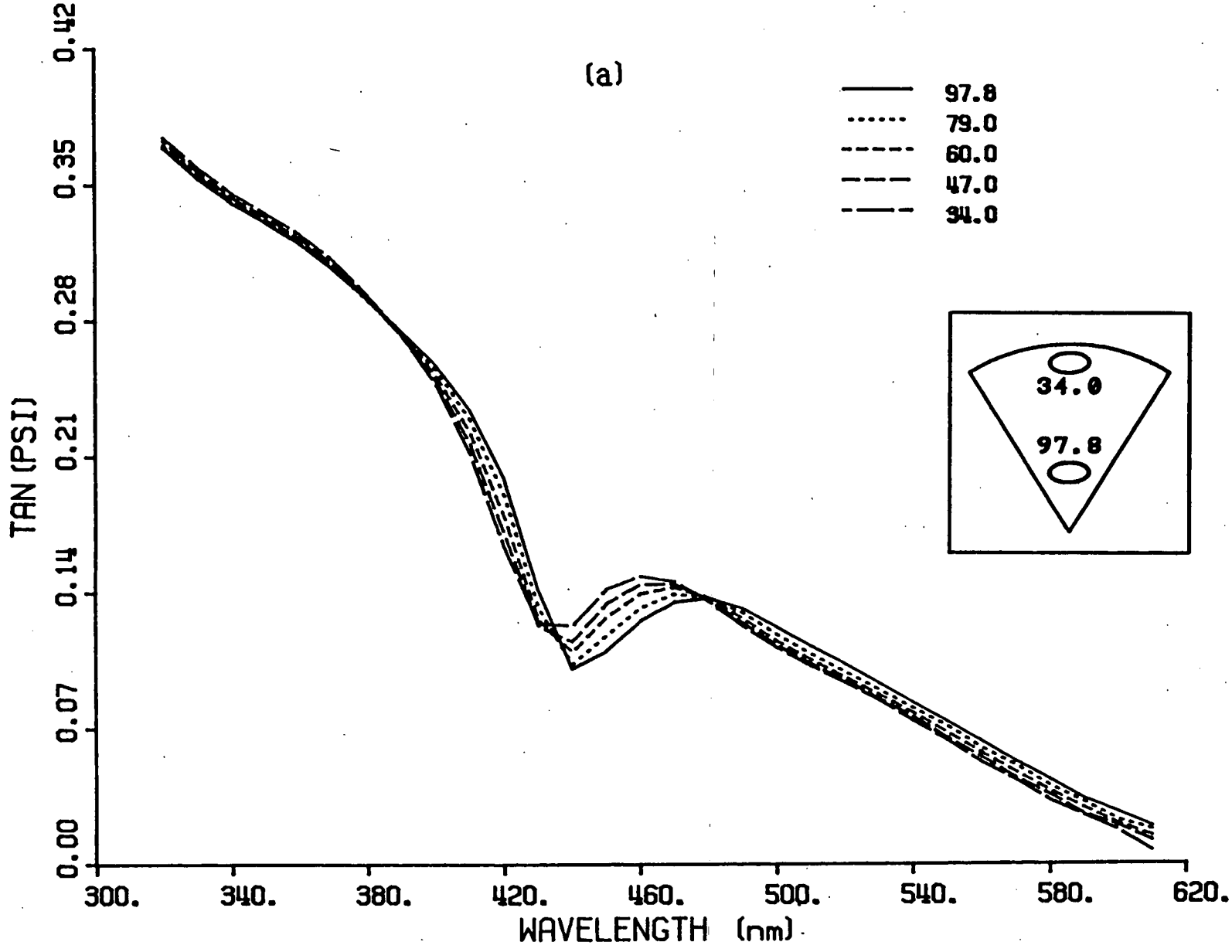
(a)
97.8
79.0
60.0
47.0
34.0
34.0
97.8
TAN (PSI)
0.00
0.07
0.14
0.21
0.28
0.35
0.42
300.
340.
380.
420.
460.
500.
540.
580.
620.
WAVELENGTH (nm)

Fig 10a

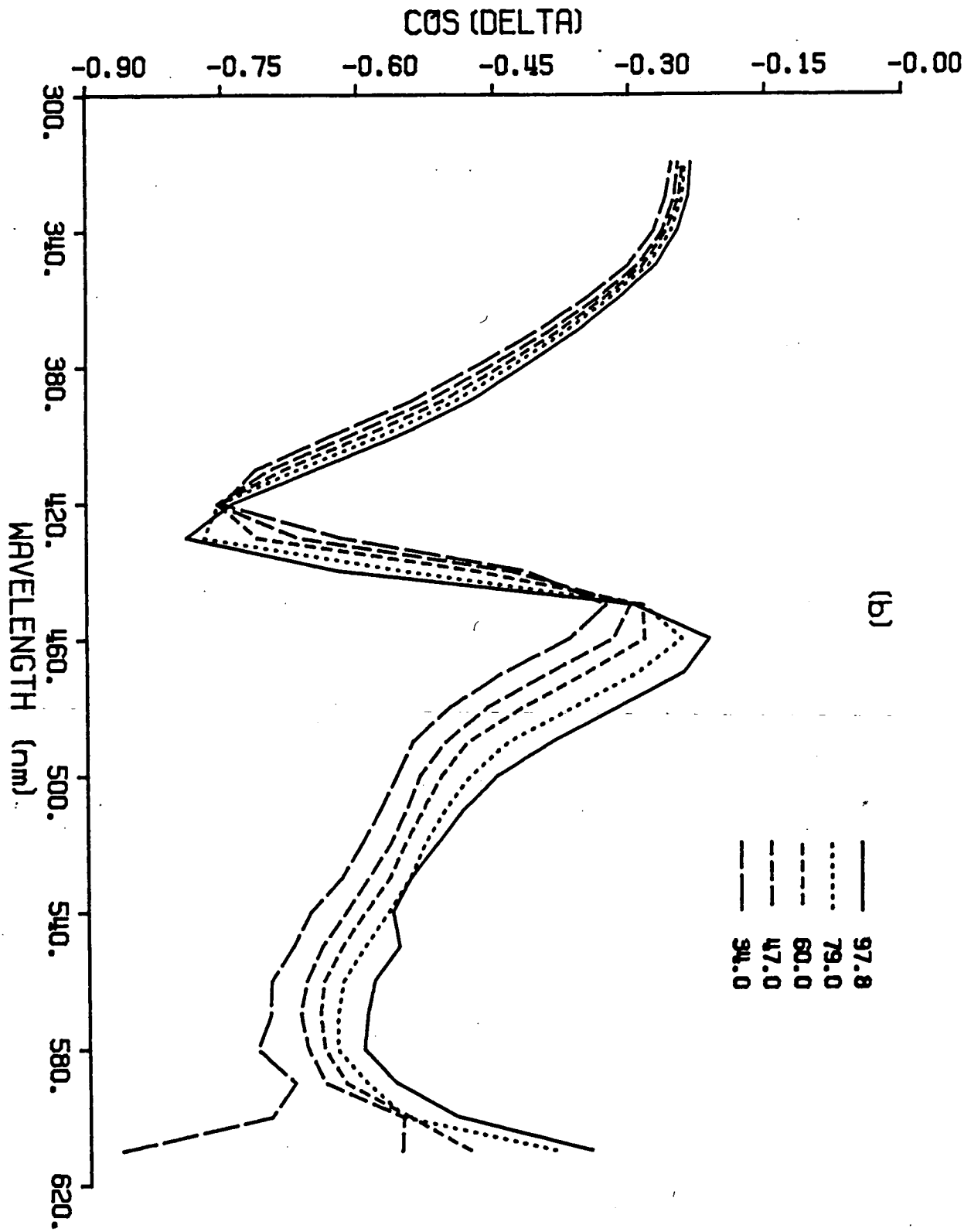
COS (DELTA)
-0.90
-0.75
-0.60
-0.45
-0.30
-0.15
-0.00
300.
340.
380.
420.
460.
500.
540.
580.
620.
WAVELENGTH (nm)
(b)
34.0
47.0
60.0
73.0
97.8

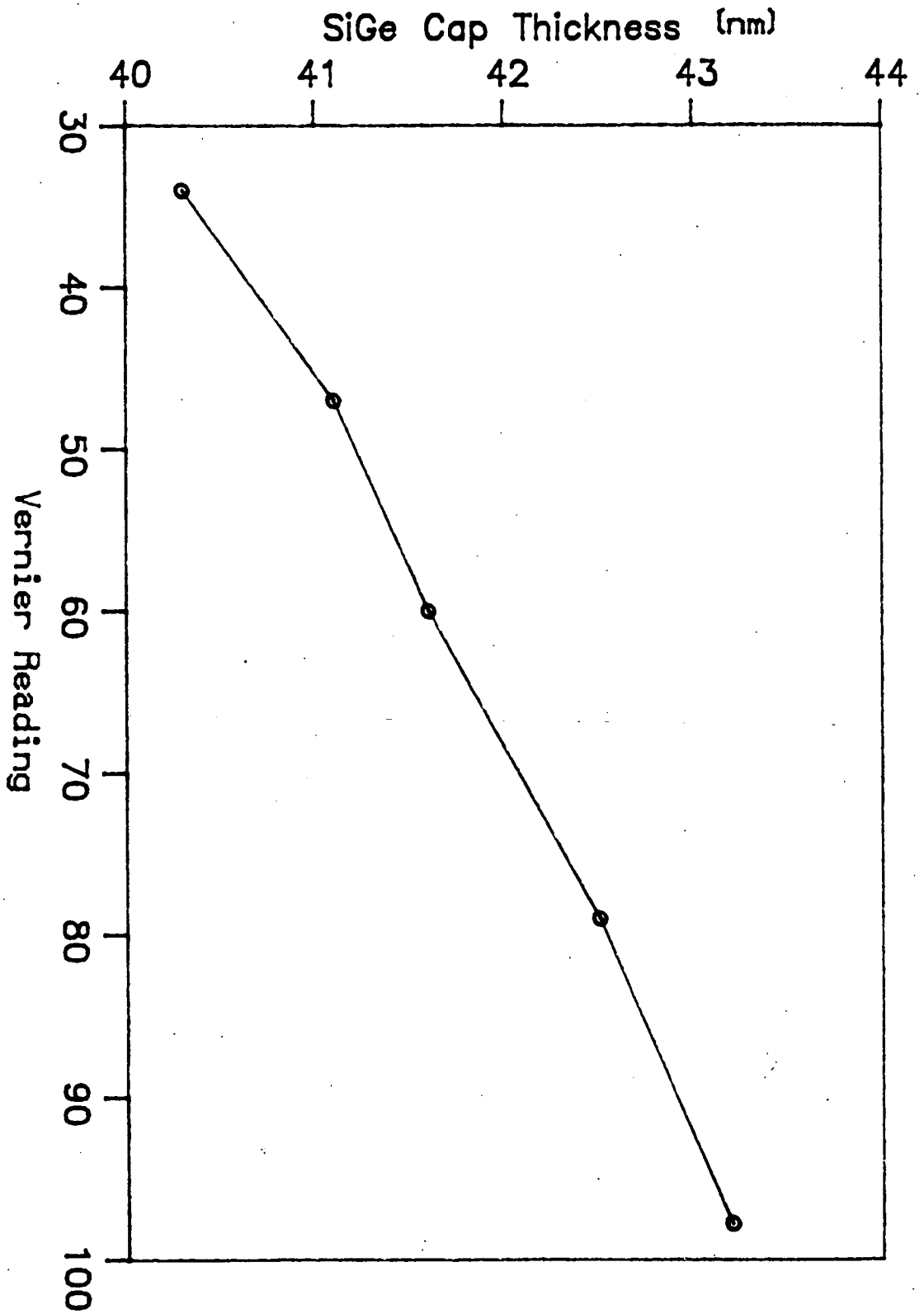
SiGe Cap Thickness (nm)
40
41
42
43
44
Vernier Reading
30
40
50
60
70
80
90
100

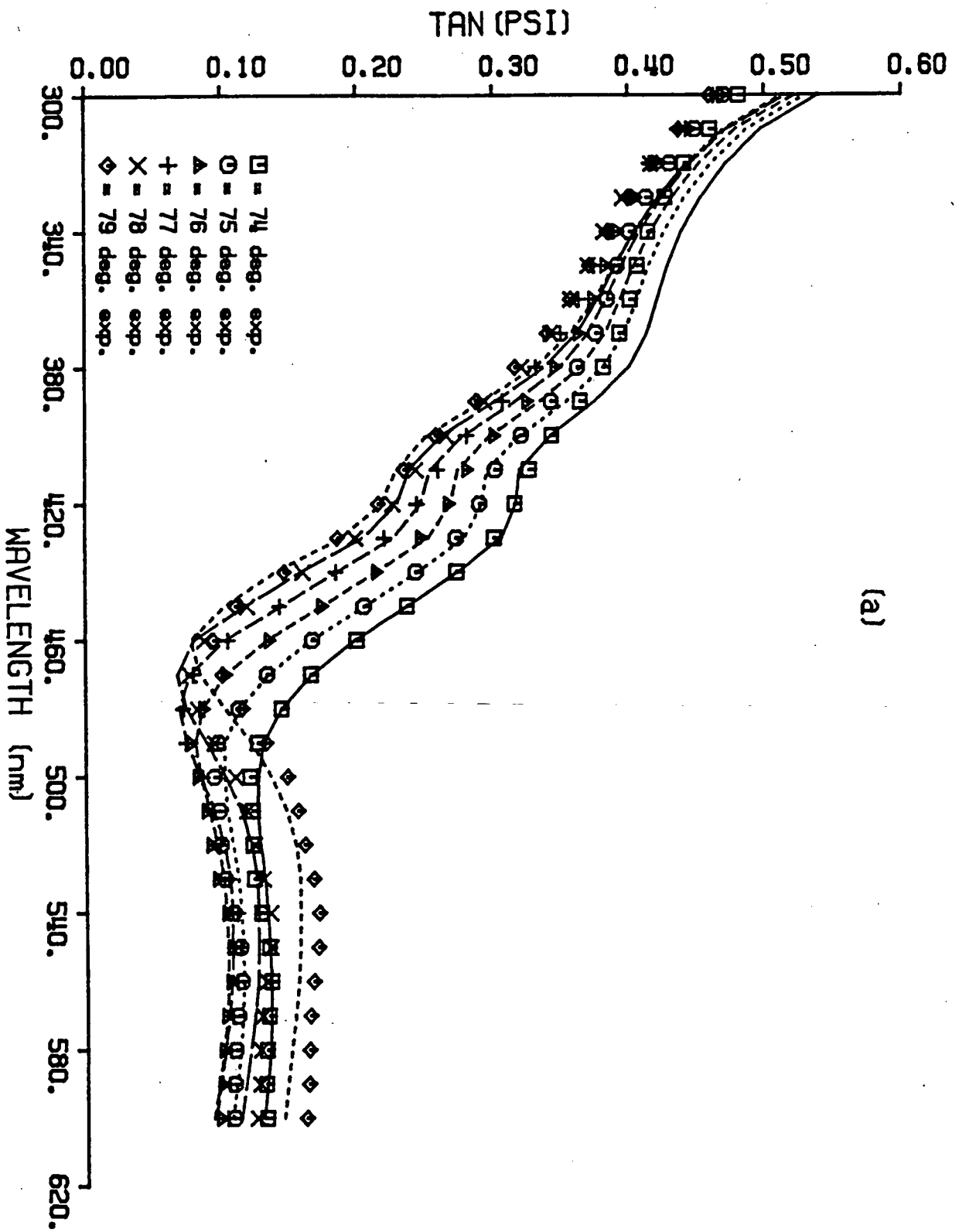
TAN (PSI)
0.00
0.10
0.20
0.30
0.40
0.50
0.60
300.
340.
380.
420.
460.
500.
540.
580.
620.
WAVELENGTH (nm)
exp. 74 deg.
exp. 75 deg.
exp. 76 deg.
exp. 77 deg.
exp. 78 deg.
exp. 79 deg.
(a)

Fig 12a

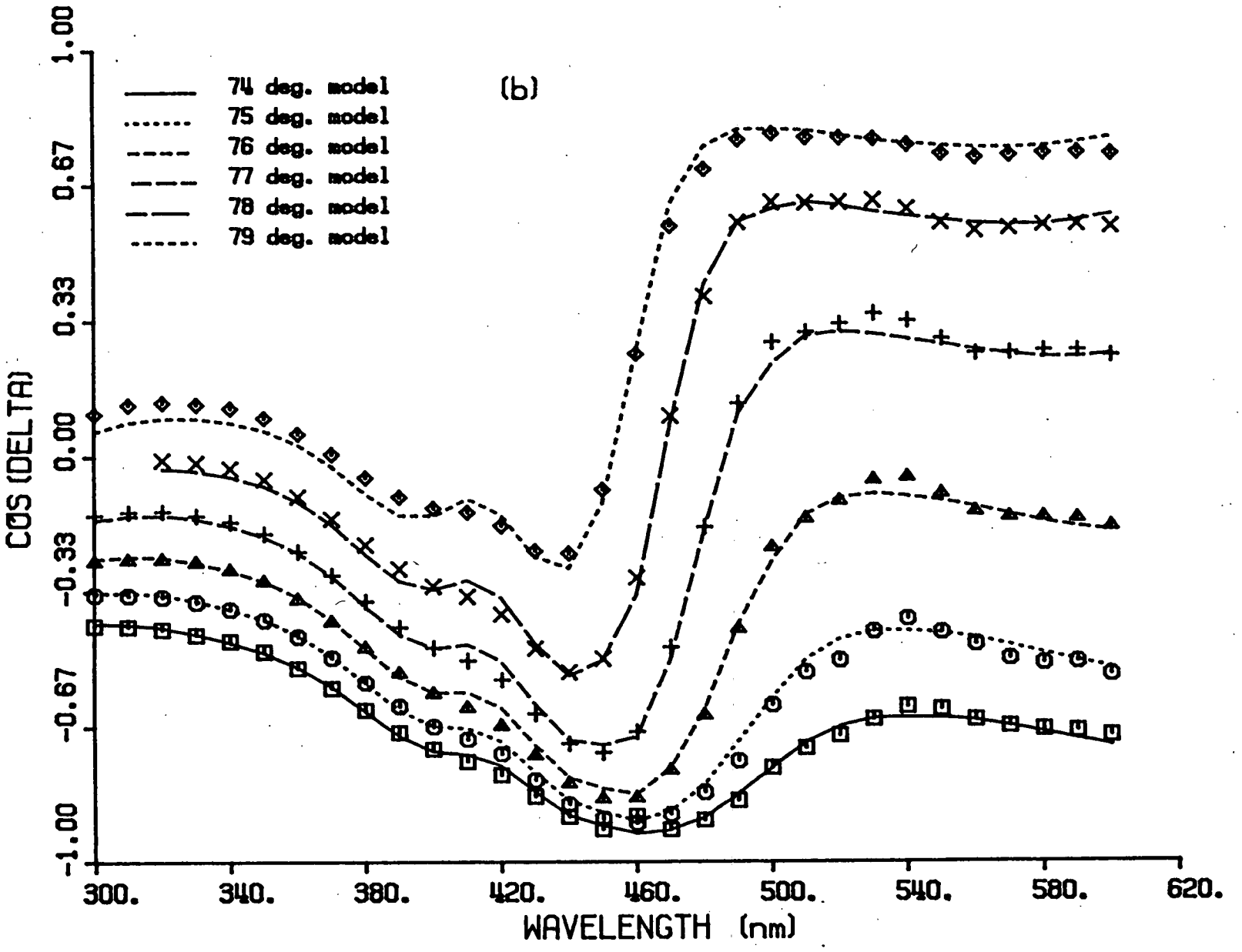
74 deg. model
75 deg. model
76 deg. model
77 deg. model
78 deg. model
79 deg. model
(b)
COS(DELTA)
1.00
0.67
0.33
0.00
-0.33
-0.67
-1.00
300.
340.
380.
420.
460.
500.
540.
580.
620.
WAVELENGTH (nm)

Fig 12b